Heliyon

Received:
18 June 2015
Revised:
12 August 2015
Accepted:
20 October 2015

Heliyon (2015) e00039

Dark rotors in the late universe

Frederick J. Mayer *

Mayer Applied Research Inc., 1417 Dicken Dr., Ann Arbor, MI, United States

* Corresponding author.
E-mail address: fmayer@sysmatrix.net.

Abstract

The tresino phase-transition that took place about 300 years after the big-bang, converted most baryons into almost equal numbers of protons and tresinos. Many of these become oppositely-charged rotating pairs or "rotors". This paper examines the formation, evolution, disposition and observations of the protons and tresinos from the phase-transition to the present era. The solar corona is further examined within the same tresino phase-transition picture.

Keywords: Cosmology, Dark matter, Solar corona, Dust extinction

1. Introduction

It is well-documented that the Standard (ΛCDM) Model of cosmology (see e.g., Weinberg [1]) has two large and undefined mass-energy components "dark matter" and "dark energy". The Standard Model also requires a number of somewhat arbitrary parameters to "fit" observed data from the cosmic microwave background (CMB). In addition, connections to other areas of physics research, other than cosmology, seem slight or non-existent. For these and other reasons my (late) colleague John Reitz and I started examining whether a class of particles (*tresinos*) that appeared to resolve some paradoxes in other physics research areas, e.g., in geophysics (discussed in by us in Mayer & Reitz [2]) and in the solar corona (first discussed in Mayer & Reitz [3]), might be involved in the "strangeness" of the Standard Model. These studies resulted in our tresino phase-transition "big-bang" cosmology. The tresino-transition cosmology, has all of the mass-energy components defined. Furthermore, it connects to a number of late-time astrophysical observations as I detail in this paper.

http://dx.doi.org/10.1016/j.heliyon.2015.e00039
2405-8440/© 2015 The Author. Published by Elsevier Ltd. This is an open access article under the CC BY-NC-ND license (http://creativecommons.org/licenses/by-nc-nd/4.0/).

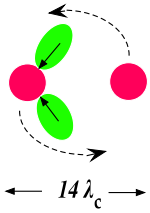

Figure 1. A classical illustration of the PTM rotor ground-state.

In our recent paper [3] we described how the tresino phase transition, in a critically-dense universe, transforms ordinary plasma baryons (mostly protons) into negatively-charged tresinos, a roughly equal number of positively-charged protons, and a small amount (≈ 5%) of ordinary matter. Many of the tresinos and protons pair-up into rotors that, given enough time, radiatively spin-down as proton–tresino molecules (PTMs) or "dark rotors". The rotors are weakly interacting massive particles and represent our picture of "dark matter". A classical illustration of the ground-state dark rotor is shown in Fig. 1 with protons in red and tresino electrons in green (λ_c is the electron Compton wavelength). In [3], we focused on the physics of the tresino phase-transition emphasizing the effects in the early time, during and just after the phase-transition. This paper examines evolutionary aspects of the tresino–proton plasma, the formation of the dark rotors, and finally some effects that dark rotors might have upon present era astrophysical and cosmological observations. In particular, models are presented for the sizes and numbers of rotors as functions of time, z, and some astrophysical observations that can be understood due to the rotors. As we presented in [3], the association between the tresino transition late in the early universe, and in the solar corona, is further examined to better understand the tresino and proton plasmas beyond the phase-transition era.

Readers are referred to our earlier paper (Mayer & Reitz [4]) for an introduction to tresino physics and Compton composites.

2. Rotor distribution model

In [3], we associated the WMAP observation of roughly 25% of the mass-energy of the universe to the spun-down rotors having been created at $z \approx$ 103,000, i.e., much before the recombination era at $z \approx 1100$. (See Section 9 for an explanation of the observed dark rotor fraction.) Note that spun-down rotors have dimensions less than the Bohr radius. Further, we proposed that the remaining mass-energy of roughly 70% had continued-on through the recombination era as rotors with much longer spin-down times. We also showed that the radiative energy-loss of the rotors was dependent upon the impact parameters at the time of their formation. The spin-down time scaling going as $\tau_{sd} = 1.9 \times 10^{-12} d^{\,6}$ with τ_{sd} in years and d the initial impact parameter in Comptons.

http://dx.doi.org/10.1016/j.heliyon.2015.e00039
2405-8440/$ – see front matter © 2015 The Author. Published by Elsevier Ltd. This is an open access article under the CC BY-NC-ND license (http://creativecommons.org/licenses/by-nc-nd/4.0/).

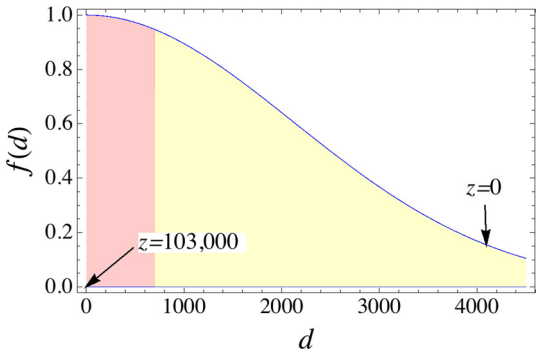

Figure 2. The model rotor distribution as a function of the initial impact distance d in Comptons. The start of the transition ($z \approx 103{,}000$) and the present ($z = 0$) are also indicated.

To further characterize the rotor population, a simple impact parameter distribution model was chosen; specifically, a normalized Gaussian distribution of rotor impact parameters,

$$f(d) = (2/\sqrt{\pi} d_s)\, e^{-(d/d_s)^2} \tag{1}$$

where d_s is a scale factor that has been adjusted such that about 25% of the rotors lie within the region $0 \leq d \leq 700$. With this choice, it is straightforward to find that $d_s \simeq 3000$. Fig. 2 presents this model distribution, where the pink region represents those rotors that have spun-down before recombination and the yellow region those rotors that are still spinning-down after recombination, or are otherwise dispersed (see Section 9). Other distribution functions produce similar results when fit in this way. For later reference, note that $z = 0$ for this model distribution obtains at $d = 4134$; more is said about this below. Finally, note that with the assumed distribution, from integrating the number of rotors beyond $z = 0$, there may be some rotors ($\approx 5\%$) that have not yet fully spun-down. The reader should note that this picture of rotor distribution has assumed that all of the tresinos and protons have undergone collisions, hence forming rotors close to the transition time. However, as I show below in Section 9, many of the tresinos and protons may have found a different fate in the expanding universe.

3. Late-time rotors

Begin by considering the spin-down time scaling as a function of z. Using the scaling derived in Section 5.1 of [3], $B_0 \propto r^{-3}$ scaling, and with the time-to-z conversion for the critically-dense universe, after resetting the "zero" of time to the transition at $z \approx 103{,}000$, the rotor diameter as a function of z can be determined. This straightforward calculation results in the formula below,

$$d = d_{tr} - \alpha\,[\beta + \gamma\,(1+z)^{-3/2}]^{1/6} \approx d_{tr} - 4134\,(1+z)^{-1/4} \tag{2}$$

2405-8440/$ – see front matter © 2015 The Author. Published by Elsevier Ltd. This is an open access article under the CC BY-NC-ND license (http://creativecommons.org/licenses/by-nc-nd/4.0/).

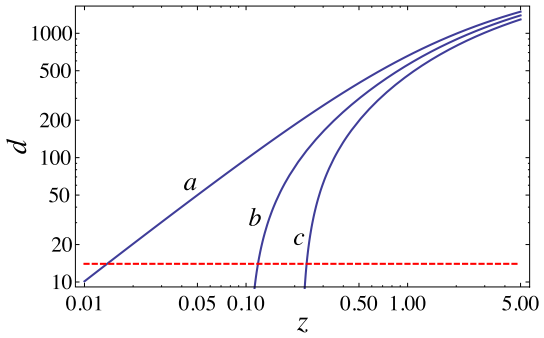

Figure 3. Rotors that have been formed at three different initial impact parameters: (*a*) $d_{tr} = 4134$, (*b*) $d_{tr} = 4034$, and (*c*) $d_{tr} = 3934$. The dashed red line indicates the rotor's minimum radius, i.e., those that have spun-down to the rotor's ground state.

where d_{tr} is the rotor's initial impact parameter (in Comptons) at the time of the tresino transition; the parameters in Eq. (2) are: $\alpha = 90.1$, $\beta = -283$ (this term is set to zero in the approximate form), and $\gamma = 9.35 \times 10^9$. Now, using Eq. (2), it is possible to examine the rotors that have, or have not, completely spun-down prior to times closer to the present. Note that only a few rotors, those with the very largest initial impact parameters, are still spinning-down to become proton–tresino molecules (rotors). However, as we suggested in [3], new rotors can be generated at the surface of the (ordinary matter) stars, so in the interstellar medium, it is to be expected that there will be some combination of dark rotors, some from late in the early universe, and some from the on-going conversion of ordinary matter to dark matter at stellar surface (see Section 8).

There surely was a spectrum of initial impact parameters, so observing the rotors at some particular z, there still would be a distribution of rotors with different radii. For example, in Fig. 3, drawing a vertical line at, say $z = 0.4$, a number of rotors of different diameters would be encountered. This is especially important at low-z's as is clear from Fig. 3. Finally, note that the different rotor sizes will complicate extracting luminosity data from distant objects (see Section 7).

4. Dark rotors in interstellar space

To begin, recall that only a small percent of the universe is composed of ordinary matter, most of the baryons having been converted, by the tresino phase transition, into proton–tresino pairs (dark rotors). Therefore, it would be expected that there were astrophysical observations produced by this large amount of the interstellar dark matter. In [3], we showed that some of the ubiquitous "unidentified infrared bands" could be associated with re-radiation from rotors that had been spun-up by local energetic stellar sources. In contrast, this section focuses upon possible astrophysical observations of dark rotors in absorption (or extinction).

2405-8440/$ – see front matter © 2015 The Author. Published by Elsevier Ltd. This is an open access article under the CC BY-NC-ND license (http://creativecommons.org/licenses/by-nc-nd/4.0/).

4.1. Continuous background extinction

It has been known for decades, that interstellar "dust" presents difficulties in extracting information from many astrophysical observations. The reader in referred to the review article by Draine [5], who presents various interstellar dust models and their associated problems. Many models employ very small hydrocarbon and/or silicate particles as the absorbers of interstellar radiation. It is useful to examine a typical extinction curve in some detail. Fig. 3 presents an average interstellar extinction curve reproduced from the data in a classic paper of Savage & Mathis [6]; it extends through the visible from far infrared to the far ultraviolet. The prominent features are the extinction bump at about 5.7 eV and the rising background extinction as the photon energy increases through the ultraviolet. These features might be explained as a result of the spun-down dark rotors in our local neighborhood in the present era whereas the small extinction spikes in the infrared are associated with the rotational levels of the entire rotor as discussed in emission in [3].

Draine comments that "the pronounced increase in extinction as the wavelength changes from visible to vacuum ultraviolet cannot be accomplished without a large population of very small grains, with sizes $a \leq 0.02$ μm" where a is the dust particle radius. This is so because the extinction scaling of the cross-section goes as: $C_{ext} \propto 8\pi^2 a^3/\lambda$ (see Bohren & Huffman [7] pg. 140). The rotor's ground state radius (see [3]) is about 4×10^{-10} cm, a value that easily satisfies Draine's size criteria. Furthermore, note that (a) the rotors are expected to be very numerous, representing a large fraction of the mass in the universe (if distributed uniformly), hence they are much larger in numbers than are atoms and molecules, and (b) they are small on the scale of atoms and molecules. Rotors may then be expected to act as extinction centers of interstellar radiant flux.

4.2. The 2175 Å extinction line

This feature has been well studied in many astrophysical observations over the past few decades. It has been observed to be a quite stable component of interstellar measurements (Fitzpatrick & Massa [8]). These authors found that this line varies by less than 1% and the line width by less than 20%. This remarkable consistency has made dust modeling difficult as Draine has pointed out.

Now, consider the rotors as the "carriers" of the extinction line. To begin, recall that energy levels of the rotors, from [3], are given by,

$$E_n = \frac{0.325\, E_0}{n}$$

2405-8440/$ – see front matter © 2015 The Author. Published by Elsevier Ltd. This is an open access article under the CC BY-NC-ND license (http://creativecommons.org/licenses/by-nc-nd/4.0/).

where $E_0 = 3700$ eV is the Compton energy unit. So, the energy required to excite the next rotational level is,

$$\Delta E_n = \frac{0.325\, E_0}{n} - \frac{0.325\, E_0}{n+1}.$$

Taking the rotor ground state as $n = 14$ results in an energy to excite the first rotational energy level $\Delta E = 5.72$ eV or 2171 Å. As we noted in [3], the smallest rotor (PTM) diameter (the "ground state") was $d \approx 14.8$ Comptons as determined from fitting the infrared emission spectra. Therefore, the extinction at the peak of the line agrees reasonably well with the emission observations. But understanding the width of this extinction line is important and is examined next.

4.3. Rotor extinction model

The extinction of light by small particles has been detailed by Bohren & Huffman [7] in their Chapter 5. In particular, use is made of their Eq. (5.18) to derive an extinction cross-section model. In a first simplified model, the rotors will be considered to be spheres.

The extinction cross-section (see Bohren & Huffman [7] Eq. (5.18)) can be written,

$$\sigma_{ext} = 8\pi^2(a^3/\lambda)\mathrm{Im}(\alpha) \tag{3}$$

with $\mathrm{Im}(\alpha)$ written as,

$$\mathrm{Im}(\alpha) = 3\epsilon''/(2+\epsilon')^2 \tag{4}$$

where ϵ' and ϵ'' are the real and imaginary parts of the dielectric function of the rotors, respectively. The medium in this case is "free-space" with $\epsilon' = 1$, as is the real part of the rotor's dielectric function. The imaginary part of the rotor's dielectric function represents the absorption throughout the optical spectrum.

A Lorentz (or natural) line-shape model is used to examine the width of the resonant extinction line. The normalized Lorentz line profile (see Rybicki & Lightman [9]) is given by,

$$\epsilon'' = \phi_\nu = \frac{\Gamma}{4\pi^2(\nu-\nu_0)^2 + (\Gamma/2)^2} \tag{5}$$

where Γ is the damping constant in a Drude model, and where ν_0 is the line center. In the case of a quantum jump between the two adjacent rotor levels the damping is quantum mechanical, a result of the Heisenberg uncertainty principle broadening the resonance. The rotor's ground-state is expected to be rather broad due to the complex electromagnetic interaction between the proton, as it orbits the tresino, with the dipole magnetic fields of its bound electrons.

2405-8440/$ – see front matter © 2015 The Author. Published by Elsevier Ltd. This is an open access article under the CC BY-NC-ND license (http://creativecommons.org/licenses/by-nc-nd/4.0/).

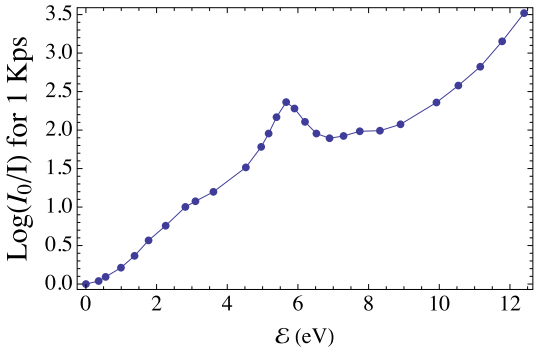

Figure 4. An average extinction curve (for one kilo-parsec) as a function of photon energy (eV), points have been joined to guide the eye.

It is now possible to write down the form of the extinction function by substituting Eq. (4) into Eq. (3) and converting to frequency and to energy with ν in electronvolts (eV)

$$\log[I_0(\nu)/I(\nu)] = n_{rot}\,\sigma_{ext}\,L \tag{6}$$

for a one kiloparsec path to compare it to the average extinction curve of Fig. 4. In Eq. (6), n_{rot} is the number density of rotors, σ_{ext} is the extinction cross-section, and $L = 3 \times 10^{21}$ cm is the one kiloparsec path length.

4.4. Comparing the extinction model and data

Now it is possible to compare the extinction model to the data presented in Fig. 4. First, taking $\nu_0 = 5.72$ eV and taking the ground-state rotor radius to be $a_{gs} = 0.77\, n_{gs}\, \lambda_c$ with $n_{gs} = 14$ to find $a_{gs} = 4.1 \times 10^{-10}$, about a factor of ten smaller than the Bohr radius. Using these values, a least-squares fit is made over the wavelength region of Fig. 4, noting that there is only one adjustable parameter in the model, namely the damping constant Γ. The best fit for the ground-state only model is shown as the red curve in Fig. 5.

A two-level rotor model was also examined by taking separate rotor densities and cross-sections as $(n_{gs}\sigma_{gs} + n_1\sigma_1)$ L using both the ground-state level and the next rotor level. This second level ($n = 15$) has $\nu_0 = 5.01$ eV and $a_1 = 4.39 \times 10^{-10}$ cm and again a least-squares fit made over the spectrum. In the two-level rotor case, it was found that the ground-state fraction was 41% and the second level was 59%. Other data from this minimization gave: $n_{gs} = 3.04$ and $n_1 = 6.5$ along with the separate damping constants, $\Gamma_{gs} = 4.1$ and $\Gamma_1 = 12$. The green curve, in Fig. 5, is the least-squares fit to the two-rotor level model. Note that this model is a somewhat better fit across the two-resonances than is the one-resonance model. This is due to the second-levels slightly lower resonance energy. In both models, a

http://dx.doi.org/10.1016/j.heliyon.2015.e00039
2405-8440/$ – see front matter © 2015 The Author. Published by Elsevier Ltd. This is an open access article under the CC BY-NC-ND license (http://creativecommons.org/licenses/by-nc-nd/4.0/).

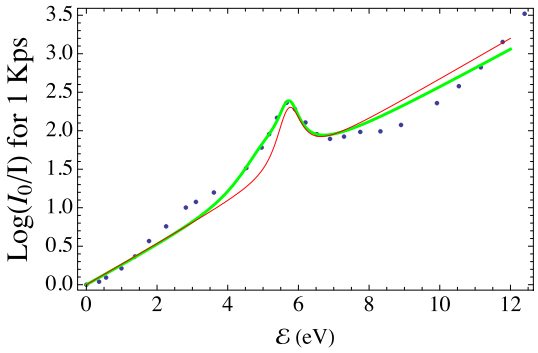

Figure 5. The least-squares data fits to the model: the red curve has $\Gamma = 4.4$ and $n_{rot} = 6.7$. The measured data (as in Fig. 4) with points not connected. Also shown is the two rotor-level, least-squares fit curve in green. See the text for other fit parameters.

single rotor level, and the two level models, the rotor densities are comparable at 6.7 and 10 cm^{-3}, respectively.

The two-level fit appears to be somewhat better than the single-level fit. This suggests that the first level is still spinning-down; this is consistent with the results presented in Section 3. Furthermore, note in Fig. 5 that the measured extinction is low compared to the model at energies between about 7 eV and 12 eV, and it is too high below about 4 eV. This is not unexpected if the rotors are responsible for the extinction line because at the higher energies there are no rotor levels, they all lie below the first energy level. This is so because the energy levels difference scales as $\Delta E_n \propto E_0/(n + 3n^2)$ (see Section 5.2 of [3]). Of course, this data fitting exercise does not verify our rotor model of the extinction, but it represents a clear alternative to the very small atomic composition most-often suggested.

Turning now to the damping constants Γ; the damping results from the rotor's ground and first rotational level being broadened by the Heisenberg uncertainly relation. The time-scale from the broadening can be estimated as $\Delta t \approx \hbar/\Gamma \approx 1.6 \times 10^{-16}$ s. That this is the relevant time-scale can be seen by comparing it to the rotors period of revolution, τ. For the ground state, τ is approximately 1.3×10^{-16} seconds, so $\tau/\Delta t \approx 1$, thus satisfying the uncertainty relation within only a few rotations.

5. Dark rotor halo

It is now useful to compare the rotor density, obtained from the extinction data fit with other characteristic densities. With our tresino transition picture it is possible to estimate the rotor density that would be observed at $z = 0$ assuming (unrealistically) there had not been any late-time, non-uniform, gravitational effects. This density would have been approximately 2.7×10^{-6} cm^{-3} thus

2405-8440/$ – see front matter © 2015 The Author. Published by Elsevier Ltd. This is an open access article under the CC BY-NC-ND license (http://creativecommons.org/licenses/by-nc-nd/4.0/).

indicating, if the estimates of the rotor density from extinction-fits are even close to being correct, that a considerable densification of the rotors must have taken place during the evolution of the our Milky Way galaxy.

A second useful comparison is to the galactic average proton density. Taking typical estimates of the mass and dimensions of our galaxy and assuming all of the matter to be protons, the density would be about 3000 protons cm^{-3}. In this case, the rotor density is only a small fraction of the galactic average proton density. So, the rotor density inferred from the extinction data is much larger than its early universe value but much smaller than the average proton galactic density.

Given the rotor density from the above extinction fits (see Section 4), it is straightforward to calculate that, if the rotors were distributed uniformly within the observable Milky Way mass, it would amount to only about 6% of the galaxy mass, i.e. considering only the visible galaxy mass. If, on the other hand, the rotors were distributed in a uniform sphere, as has been suggested before (see e.g., Evans [10]), with a radius $1.2 \leq R/R_{Gal} \leq 1.5$ then the ratio of rotor mass to galaxy mass would be between 10 and 20. So, assuming the rotors are the "carriers" of the extinction observations as was done above, they would then have to populate a very large volume surrounding our galaxy. Of course, it would be expected that the density of rotors was somewhat higher at the center and decreasing at larger distances by gravitational equilibration (e.g., see Navarro, et al., [11]).

Finally, it is instructive to consider a crude dark rotor gas "halo" by making use of one of Chandrasekhar's analytic gaseous stars ([12] pg. 231). In particular, a star with radiation as a fraction of the total pressure supporting it and use the estimate of the dark rotor gas density (see Section 4) to determine a mean rotor gas temperature. Assume that the spherical dark matter (rotor gas) halo is centered upon and encloses our Milky Way galaxy; the halo is gravitationally balanced by the pressure of the rotor gas and radiation. Note that this crude model neglects the effects of rotational velocity of the halo gas. Taking the dark rotor density to be about 10 cm^{-3} from above (from Section 4), it is straightforward to calculate the halo radius in units of the Milky Way radius giving $R_{Halo} = \eta\, R_{Gal}$, where η is a multiple of the galaxy radius. Now, using Chandrasekhar's Eq. (68) the mean rotor gas temperature is found to be $\bar{T} \approx 1.3\, \beta\, \mu\, \eta^2$ keV, where β is the fraction of total pressure due to the rotor gas, and $\mu = 2$, is the rotor's atomic mass. If the halo is primarily supported by the rotor gas, then β is close to one. So, $\bar{T} \approx 2.6\, \eta^2$ keV or perhaps somewhat less if rotational energy and radiation are important. Finally, note that galactic rotational kinetic energies in this case would then be comparable to rotor gas temperatures of a few keV (e.g., see Navarro, et al., [11]).

Given the rotor gas temperature estimate, it is possible to examine the effects of rotor–rotor collisions.

 http://dx.doi.org/10.1016/j.heliyon.2015.e00039
2405-8440/$ – see front matter © 2015 The Author. Published by Elsevier Ltd. This is an open access article under the CC BY-NC-ND license (http://creativecommons.org/licenses/by-nc-nd/4.0/).

6. Dark rotor self-interactions

The mean rotor gas temperature could affect the survival of the rotors during rotor–rotor collisions. In this section, a simple collision model of the self-interactions and rotor survivability are presented.

The reader will recall that dark rotors are composed of electromagnetically bound protons and tresinos. These two components are bound at about the few hundred eV energy level whereas the tresino with its two electrons and one proton are electromagnetically bound together at the 3.7 keV energy level. Direct collisions between two rotors is most likely to interrupt the proton–tresino (rotor) bond much more frequently than to disassemble the tresino into its constituent components. If the latter happens at keV center-of-mass energies, the electrons and protons may then be converted into ionized hydrogen plasma and eventually reassemble into neutral hydrogen. In the case that the collision breaks the proton/tresino bond, the two components will most likely reform into a rotor because of their electrostatic attraction bringing them back together, similar to the process by which they were initially formed late in the early universe. In the latter case, a new cycle of rotor spin-down will begin again with its attendant low-energy radiative energy loss.

6.1. Rotor collision rate

A conservative estimate of the collision cross-section is to consider the rotors as "hard spheres" so that $\sigma_{r_a,r_b} \approx \pi(r_a^2 + r_b^2)$ for the two colliding rotors with radii $r_{a,b} \geq 7\,\lambda_c$, resulting in $\sigma_{r_a,r_b} \geq 4.4 \times 10^{-19}$ cm^2. The cross-section for direct impact of the tresinos of the two rotors (classically speaking) would be considerably smaller due to their smaller dimensions. Taking the rotor gas temperature to be 5 keV and also 10 rotors/cm^3, then a rotor–rotor collision rate of about 2×10^{-9} collisions/s-cm^3 or roughly one collision/cm^3 every 16 years. But as mentioned, reformation of rotors is expected to maintain their numbers while only slowly changing the background temperature.

7. Supernovae and the accelerating universe

We stated, in [3], that our critically-dense cosmology was not consistent with an accelerating universe. The primary observations supporting an accelerating universe were the measurements of distant supernova explosions that appeared to be less luminous than would be expected at their observed distance. These data and certain theoretical arguments required there to be some type of energy called dark energy, with a still on-going research to understand what this energy could be. At

 http://dx.doi.org/10.1016/j.heliyon.2015.e00039
2405-8440/$ – see front matter © 2015 The Author. Published by Elsevier Ltd. This is an open access article under the CC BY-NC-ND license (http://creativecommons.org/licenses/by-nc-nd/4.0/).

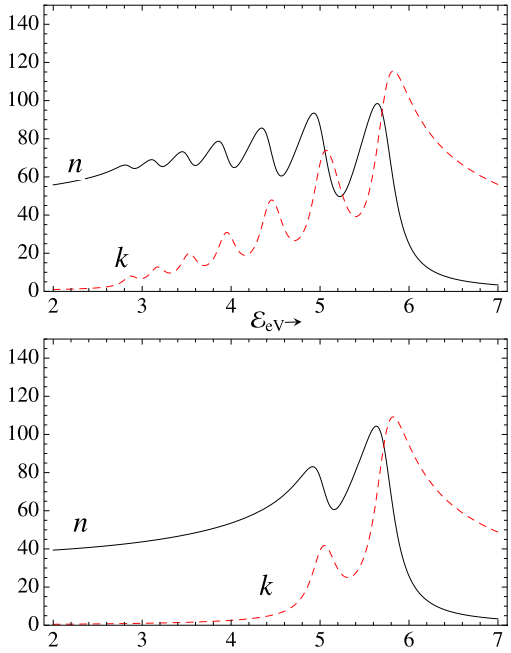

Figure 6. The upper plot shows the optical constants, n and k, the real and imaginary parts of the refractive index as a function of photon energy in the case of seven resonances. The lower plot shows the optical constants for the case of just two resonances, as occurs much later in time.

the time that [3] was written, we had not yet understood the effects of the late-time rotor extinction might have upon the supernovae observations. However, since then it has become clear that the rotor extinction is quite important. This section presents a model calculation of the extinction of the supernovae luminosity due to the long-lived rotors still spinning-down at $z \leq 7$. For the sake of clarity, the discussion that follows begins by looking at the resonances in the gas of rotors through which light from an embedded supernova must pass on its way to us.

Fig. 6 presents two plots of rotor gas resonances of prolate spheroidal shape (see Bohren & Huffman [7] Section 5.3) using a multiple-oscillator model (see Bohren & Huffman [7] Section 9.2). The plots of Fig. 6 present the results for the seven-resonance transitions (see Section 4.2 above) specifically, resonances at 5.72, 5.01, 4.42, 3.92, 3.52, 3.16, and 2.86 eV in the upper plot, and just two resonances at 5.72 and 5.01 eV in the lower plot. Note that the first resonance at 5.72 eV is the transition from the rotor's ground-state to the first rotational state (see Section 4). There are many other lower energy resonances as well, but these rotors will have spun-down at much earlier times in the late universe. The plots in Fig. 6 are presented in the rest frame and will, of course, be red-shifted down to $z = 0$. Importantly, these resonances are spread across the visible spectrum. Also, given the optical constants, it is straightforward (see Bohren & Huffman [7], pg. 227) to

 http://dx.doi.org/10.1016/j.heliyon.2015.e00039
2405-8440/$ – see front matter © 2015 The Author. Published by Elsevier Ltd. This is an open access article under the CC BY-NC-ND license (http://creativecommons.org/licenses/by-nc-nd/4.0/).

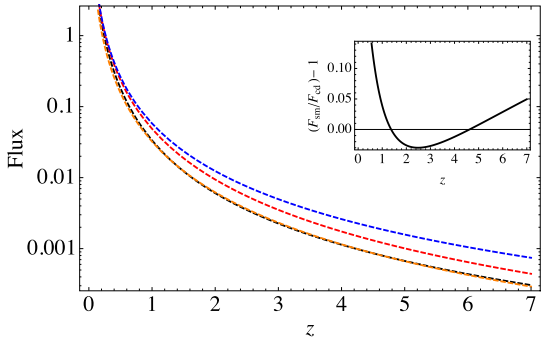

Figure 7. Comparing model fluxes, F_{sm} in dashed-black, and the best-fit F_{cd} in dashed-orange; the two are nearly indistinguishable on this scale. The inset shows the two fluxes are close to equal over the $1 \leq z \leq 7$ interval. Two other cases (in dashed-blue and dashed-red) are also shown with details in the text.

show that this gas of rotors is highly reflective of light in this band from a supernova imbedded within this gas.

From an examination of Figs. 6 & 3, it is obvious that understanding the resonance populations at small z is required to determine the attenuation of the supernovae light. This is accomplished using Eq. (2): setting $d = 14$, $d_{tr} = f\ 1434.2$, and solving for f gives $f = 0.0034 + (1+z)^{-1/4} \approx (1+z)^{-1/4}$. So, the rotor density at small z is proportional to the factor $(1+z)^{-1/4}$ and the supernovae luminosity viewed at $z = 0$ is expected to be reduced by about this factor.

It is possible now to compare the fluxes calculated using the luminosity distances for the Standard Model without rotor attenuation, and our critical-density model having $\Omega_M = 1$ with rotor attenuation. The fluxes in these models can be written,

$$F_{sm} = \frac{S}{4\pi D_{Lsm}^2} \quad \text{and} \quad F_{cd} = \frac{Sf}{4\pi D_{Lcd}^2}$$

where S is the supernovae intensity; the D_L's are the respective luminosity distances for the two models; f is the attenuation factor (noted above) due to the rotors still spinning-down at late time. The respective luminosity distances are computed and displayed in Section 7.1 below.

Now, given the luminosity distances from Section 7.1, a number of flux calculations are compared in Fig. 7, taking $S = 1$. The Standard Model flux is shown in dashed-black. The critical density model is shown in dashed-blue with $f = 1$ (i.e., no attenuation). The critical-density model with $f = (1+z)^{-1/4}$ is shown in dashed-red, and finally the critical-density model with $f = 0.66(1+z)^{-1/4}$ is shown in dashed-orange where in the latter case, a correction factor $2/3$ has been introduced that brings the rotor-attenuated, critical-density model into near agreement with the Standard Model. Note that the rotor-attenuated, critical-density model and the Standard Model are fairly close to each other over

 http://dx.doi.org/10.1016/j.heliyon.2015.e00039
2405-8440/$ – see front matter © 2015 The Author. Published by Elsevier Ltd. This is an open access article under the CC BY-NC-ND license (http://creativecommons.org/licenses/by-nc-nd/4.0/).

most of the interval $1 \leq z \leq 7$ as can be seen in the inset of Fig. 7. Furthermore, the Standard Model is seen to be tens of percents larger for $z \leq 1$ compared to the critical-density model.

These luminosity comparisons are clearly not precise. However, attenuation by the dark rotors is a clear alternative to the Standard Model with its unknown dark energy.

7.1. Luminosity distances

The luminosity distances are computed and displayed in this section and Eqs. (7) & (8).

The papers of Hogg [16] and Wright [17], provide definitions for D_L the luminosity distances. Following Wright, take $D_L = \beta\ (1+z)Z(z)$ where $\beta = c/H_0$ and

$$Z(z) = \int_{1/(1+z)}^{1} da/(a\sqrt{X(a)})$$

where $X(a) = \Omega_M\ a^{-1} + a^2\ \Omega_\Lambda$ and both radiation and curvature terms have been dropped. Here, as usual, Ω_M and Ω_Λ are the mass and vacuum energy fractions of critical density, respectively.

Two special cases of interest are required. The first case is the critical-density (Einstein–de Sitter) model taking $\Omega_M = 1$ and $\Omega_\Lambda = 0$, resulting in the familiar result,

$$D_L = (1+z)(2 - 2(\sqrt{1+z}))^{-1}\beta \tag{7}$$

The second case takes $\Omega_M = 0.3$ and $\Omega_\Lambda = 0.7$ (these are roughly the values presently used in the ΛCDM Standard Model). This case can be integrated as well (with help from Mathematica©) but is rather more complicated. The result is:

$$D_L = \beta\,(1+z)(a_1 + \{(1+a_2)\,Hy(z)\,Rt(z))/(a_2 + (1+z)^{-3}) \tag{8}$$
$$Hy(z) = {}^2F_1\,[1/3, 1/2, 4/3, -a_2(1+z)^3]$$

where $Hy(z)$ is a Hypergeometric function, and $Rt(z)$ is the square root,

$$Rt(z) = \sqrt{(0.7 + 0.3(1+z)^3)(1 + a_2(1+z)^3)(1+z)^{-4}}$$

here $a_1 = -1.140667$ and $a_2 = 0.4285714$. The two luminosity distances given by Eq. (7) & (8), are used in the flux evaluations in Section 7 above.

 http://dx.doi.org/10.1016/j.heliyon.2015.e00039
2405-8440/$ – see front matter © 2015 The Author. Published by Elsevier Ltd. This is an open access article under the CC BY-NC-ND license (http://creativecommons.org/licenses/by-nc-nd/4.0/).

Figure 8. Solar corona – Image credit: Miloslav Druckmuller/SWNS.

8. Transition-driven currents and magnetic fields

In [3], we noted the similarities between the tresino transitions in the solar corona and in the early universe. This section further examines some implications of these two related transitions. In Fig. 8 the influence of streams and loops of currents starting at the base of the corona (where $n_p \approx 10^9/\mathrm{cm}^3$) and extending out many solar radii into space is quite apparent. Some of the long filaments collapse into larger filaments while others appear to get tangled or form extended loops entangled with the solar dipole magnetic field closer to the equator. These streams are the result of the tresino transition's formation of keV protons and tresinos that escape from the base of the corona (the escape kinetic energy is about 2 keV) carrying along their imbedded magnetic fields as they expand or contract under their self-forces. Note that in the case of two nearby streams of protons and tresinos moving in the same direction will repel each other whereas the same two streams moving in opposite directions will attract each other through their respective $\boldsymbol{J} \times \boldsymbol{B}$ self-forces. Both streams are acted upon by the ambient solar dipole magnetic field as well. Also note that both protons and tresinos have a very long collisional range in the very low-density corona resulting in the strongly-entangled, magnetohydrodynamic atmosphere. Such chaotic evolution is no doubt also caused by the differing hydrodynamic initial conditions at the base of the corona from which the streams originate.

Those streams that are attracted to each other have a higher probability that protons and tresinos collide at small impact distances initiating their spin-down into rotors as previously described. On the other hand, those streams that are expelled, carrying along their magnetic fields, are less likely to collide and therefore will not spin-down but continue to expand in the energetic corona plasma. Depending upon the Mach number in a given zone, some amount of the energy from the tresino transition will be carried away in the proton and tresino streams as components of

 http://dx.doi.org/10.1016/j.heliyon.2015.e00039
2405-8440/$ – see front matter © 2015 The Author. Published by Elsevier Ltd. This is an open access article under the CC BY-NC-ND license (http://creativecommons.org/licenses/by-nc-nd/4.0/).

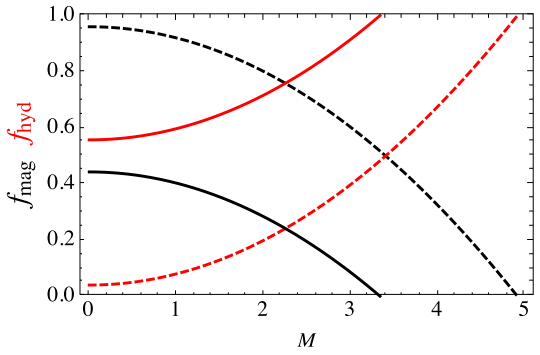

Figure 9. The fractions of hydrodynamic energy density in solid-red and the magnetic field energy density in solid-black with gravitation. The fractions of hydrodynamic energy density in dashed-red and the magnetic field energy density in dashed-black without gravitation.

the solar wind. Note that as the solar wind expands the magnetic field carried away decreases leaving behind the residual proton or tresino kinetic energy.

8.1. Magnetic and kinetic energies in a torus

The solar corona exhibits many current streams and "loops" (see Fig. 9). A simple model for the energy partitioning in these structures is now presented. Consider a torus of minor radius a and major radius R that carries a flow of collisionless protons (or tresinos) whose total number is N_p. The magnetic energy is $W_m = (1/2)L_0 I_p^2$ and the inductance is given by $L_0 = \mu_0 R(\text{Log}[8\,R/a] - 7/4)$, the current is $I_p = evN_p/(2\pi R)$ and the kinetic energy $E_k = N_p(1/2)m_p v^2$. The ratio of magnetic energy to kinetic energy is therefore,

$$W_m/E_k = e^2\,\mu_0\,N_p(\text{Log}[8\,R/a] - 7/4)/(4\,\pi^2\,m_p\,R).$$

Note that the velocity has canceled and that the ratio decreases with radius so eventually there is only kinetic energy left as the torus expands due to the $J \times B$ self-force. A straight current-carrying filament of radius a and length L gives the following similar result,

$$W_m/E_k = e^2\,\mu_0\,N_p(\text{Log}[2\,L/a] - 3/4)/(2\,\pi\,m_p\,L),$$

where again the velocity has canceled.

8.2. Magnetic and kinetic energies in the solar corona

This section presents a simple calculation of the fractions of magnetic field and kinetic energies in the solar corona. A version of the "one-zone" model presented in [3] is again revisited. The conservation of energy from the base of the corona may be written,

 http://dx.doi.org/10.1016/j.heliyon.2015.e00039
2405-8440/$ – see front matter © 2015 The Author. Published by Elsevier Ltd. This is an open access article under the CC BY-NC-ND license (http://creativecommons.org/licenses/by-nc-nd/4.0/).

$$n_c E_0 = (1 + M^2) n_c \, k \, T_c + B^2/(8\pi) + G M_\odot n_c m_p / R_\odot$$

where the subscripts c refers to the (average) values in the corona and $E_0 =$ 3700 eV is the Compton energy unit, M is the Mach number, and other quantities have their usual definitions. The term on the LHS is the tresino transition energy density at the base of the corona, the first term on the RHS is the hydrodynamic energy density, the second is the magnetic field energy density (from currents produced by the transition) and the third is the energy density required to overcome solar gravity. It is simple to evaluate the fractions representing of the three terms substituting approximate values for T_c say $\approx$ 150 eV and the relevant solar quantities to examine how these various fractions depend upon M. Fig. 9 shows the fractions of hydrodynamic and magnetic energy densities with and without the gravitational term.

The solar wind, tresino-transition driven, carrying along its currents and magnetic fields appears to be consistent with observations of the magnetic fields extending away from stars in galaxies (see Beck [13]).

It is expected that the same sort of extended, tangled, and chaotic streams and current loops would have existed at the tresino transition at $z \approx 10^5$ in the early universe, much before the recombination era. The scale-size of the magnetic energy would be expected to be comparable to the universe scale at this era and could be a larger fraction of the tresino transition energy perhaps closer to $M \approx 4$ in Fig. 9. So, in a manner similar to that of the solar corona, the magnetic field energies will also be carried away in the universe's "tresino-transition wind". However, in contrast to the solar corona transition, the early universe transition is completed in some period of time, whereas the solar corona continues so long as the Sun has sufficient protons evaporating from its surface. Assuming that the tresino transition in the early universe is similar in its effects to that of the solar corona, it is useful to inquire about the later ($z \leq 10^5$) effects upon the situation in the plasma continuing-on. Note that the plasma temperature at the time of the transition was only about 25 eV, whereas the kinetic energies of most of the expelled protons and tresinos (those that have not become rotors) after the transition was about 1.7 keV. This non-equilibrium partitioning would have persisted down to the recombination era and may well have had an impact on the observed structure formation of the later universe. Furthermore, the currents and embedded magnetic fields would be expected to expel all the protons and tresinos, those that had not previously become rotors, in extended and random patterns across the universe. In addition, these protons and tresinos will still have relatively high kinetic energies; these expelled protons and tresinos are effectively de-coupled from the remaining ordinary matter $\approx$ 5% and the rotors both of which go on to the recombination era. Whereas the ordinary matter is coupled together in the photon–baryon interactions, the energetic protons and tresinos from the transition are not. Note that there is a big difference

 http://dx.doi.org/10.1016/j.heliyon.2015.e00039
2405-8440/$ – see front matter © 2015 The Author. Published by Elsevier Ltd. This is an open access article under the CC BY-NC-ND license (http://creativecommons.org/licenses/by-nc-nd/4.0/).

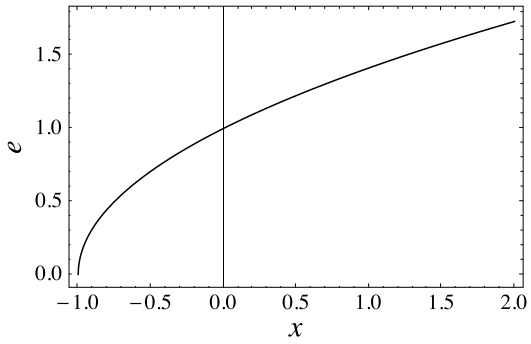

Figure 10. Eccentricity e vs x.

between the local temperature of the ordinary matter during the transition (tens of eVs) and the kinetic velocities of the expelled transition protons and tresinos (keVs). It seems natural that the extended and random distribution of transition protons and tresinos could "seed" the later development of walls and voids in the distribution of galaxies (see, for example, Geller & Huchra [14]).

Of course it can be argued that relating the tresino transitions at the corona and that of the early universe is arbitrary and there is no influence upon the early universe's later evolution. However, many observations discussed above and in [3] suggest that the tresino transition resolves many otherwise paradoxical issues. For example, the question posed by Steven Weinberg in his book (Weinberg [1], pg. 57) regarding dark energy in the Standard Model: *"why is the dark energy density comparable to the matter energy density at this particular moment in the history of the universe?"* If our tresino-transition picture is correct, then there is no dark energy, only the protons and tresinos that had been broadly dispersed after the transition. Note from Fig. 10, drawing a vertical line at $M \approx 4.4$, for the case without gravity, gives this component to be about 70% of the mass converted in the transition and about 25% having been transformed into rotors. The partitioning could therefore have existed since $z \approx 10^5$ down to the present time; the partitioning simply resulting from the collision dynamics as shown in the next Section.

9. Dark rotors as a fraction of proton–tresino collisions

Interestingly, the number of rotors may be understood from the dynamics of tresino–proton collisions. Recall that the tresino phase-transition produced protons and tresinos in roughly equal numbers each having kinetic energies of about 1.9 keV. These two particle types have closely the same mass but opposite net charge (positive protons and negative tresinos). Furthermore, because they are attracted to each other, they undergo collisions. It is useful to determine in such collisions, how many find themselves in bound elliptical (some circular) orbits.

 http://dx.doi.org/10.1016/j.heliyon.2015.e00039
2405-8440/$ – see front matter © 2015 The Author. Published by Elsevier Ltd. This is an open access article under the CC BY-NC-ND license (http://creativecommons.org/licenses/by-nc-nd/4.0/).

These collisions are well known in the two-body central-force problem (familiar in celestial mechanics) discussed in numerous textbooks (Landau & Lifshitz [15]). An essential result of the dynamics of the central (inverse-square force law, i.e., Kepler problem) can be divided by the equation for the eccentricity, e, of the orbit. This equation is:

$$e^2 = 1 + 2EL^2/\mu K^2$$

where E, L, μ are the center of mass kinetic energy, angular momentum, μ is the reduced mass (here $m_p/2$), and $K^2 = q^2$, the square of the electronic charge. Note that the collision dynamics are separated by the value of the eccentricity e: $e < 1$ for a circle or an ellipse, $e = 1$ for a parabola, and $e > 1$ for a hyperbola (see Fig. 10). Recall that the energy is negative in the case of bound states, those that become rotors.

Now, normalizing the equation for e in terms of the maximum kinetic energy in units of $E_0 = 3.8$ keV and the angular momentum in units $L = N\,\hbar$ to give,

$$e^2 = 1 + 0.3(E/E_0)N^2 = 1 + x$$

with $x = 0.3(E/E_0)N^2$. As usual, at sufficiently large N, the collisions are hyperbolic and only for small enough energies are there bound ellipses.

It is easy to compute the number of bound states by integrating $e\,n'$ where n' is the distribution of possible collisions (here assumed constant) from $x = -1$ to $x = 0$. The result is $2/3\,n'$. On the other hand, integrating $e\,n'$ from $x = -1$ to say $x = 1.5$ gives $2.635\,n'$ so the bound fraction of the collisions is about 0.25; all other collisions, outside this region, will escape. Of course a larger or smaller value of the upper integration limit will change the ratio; but this is a reasonable value. The significance of this calculation is that in the proton and tresino collisions roughly 25% become bound in either circular or elliptical orbits and are removed from the cosmic plasma whereas the others are free to expand retaining their kinetic energy. Therefore, as the cosmos continues to expand, instead of containing only the flows of protons and tresinos, it also contains the bound proton–tresino molecules (PTMs) that continue to spin-down into rotors; also roughly 75% of protons and tresinos ultimately expand, at later times, too very low densities as suggested in the previous section.

The so-called dark matter then represents all the protons and tresinos that have become bound states during collisions during and after the tresino transition that took place about 300 years after the big-bang. On the other hand, dark energy is composed of all other protons and tresinos that have not become bound and have continued to expand along with the cosmic expansion. However, the unbound protons and tresinos will expand at considerably higher speed than the ordinary matter plasma and bound rotors. Furthermore, note that these dark matter and dark

 http://dx.doi.org/10.1016/j.heliyon.2015.e00039
2405-8440/$ – see front matter © 2015 The Author. Published by Elsevier Ltd. This is an open access article under the CC BY-NC-ND license (http://creativecommons.org/licenses/by-nc-nd/4.0/).

energy fractions apply to the early universe as well as in the corona of the Sun, the latter with its clearly evident streams of charged-particles and currents (Fig. 9).

Finally it is important to realize that our dark energy (free keV protons and tresinos) have no excited states hence they are truly "dark". Our dark matter particles (the rotors) are almost completely "dark" too, except for weak extinction and rotational re-radiation (see Section 4).

10. Discussion and conclusions

This paper has shown that a number of otherwise problematic observations in astrophysics and cosmology can be resolved by understanding late-time interactions involving dark rotors, some of which may be still spinning-down after having been produced in the tresino-transition, late in the early universe.

Rotor-rotor collisions have been examined in order to consider rotor survivability in the present era. The density of dark rotors in our galaxy has been extracted from the 2175 Å resonance extinction-line assuming it is due to the almost completely spun-down rotors. The results are shown to be consistent with a large volume of low-density rotors distributed, more or less spherically, and having a length-scale larger than the dimensions of our Milky Way galaxy. It was also shown that the tresino-transition modified the expanding universe by separating the proton and tresino components into two groups, those that formed dark rotors and those that were dispersed by the self-forces of the currents and magnetic fields that may have later created sites for seeding dispersed larger-scale structures.

The connection between the tresino transition late in the early universe and that of the solar corona has been detailed further. In the tresino transition, only a fraction of the transition energy produces rotors while the remainder generates streams of keV protons and tresinos and their magnetic fields; a situation that must obtain in both cases. The solar corona may very well tell us much about the early universe phase transition.

A distribution of rotor impact parameters was introduced giving spin-down times until the present era; it reasonably accounts for the number of rotors still spinning-down. The rotors have been shown to produce a reduction of distant supernovae luminosity. With the tresino phase-transition in a critically-dense universe along with luminosity reduction of supernovae observations by the late-time rotors, there is no need for some unidentified form of dark energy. Furthermore, because the tresino-transition and critically-dense universe, accounts for all the mass in the universe, both seen and unseen (in CMB data), there is no need for some unidentified form of dark matter.

 http://dx.doi.org/10.1016/j.heliyon.2015.e00039
2405-8440/$ – see front matter © 2015 The Author. Published by Elsevier Ltd. This is an open access article under the CC BY-NC-ND license (http://creativecommons.org/licenses/by-nc-nd/4.0/).

Declarations

Author contribution statement

Frederick Mayer: Conceived and designed the experiments; Analyzed and interpreted the data; Wrote the paper.

Funding statement

The author received no funding from an external source.

Competing interest statement

The author declares no conflict of interest.

Additional information

No additional information is available for this paper.

Acknowledgements

It is with deep gratitude that I acknowledge my collaborator and dear friend Dr. John R. Reitz without whose help and encouragement this work would not have been possible. John passed away within days of the publication of our recent paper [3].

References

[1] S. Weinberg, Cosmology, Oxford University Press, Oxford and New York, 2008.

[2] F.J. Mayer, J.R. Reitz, Thermal energy generation in the Earth, Nonlinear Process. Geophys. 21 (2014) 367–378.

[3] F.J. Mayer, J.R. Reitz, Compton composites late in the early Universe, Galaxies 2 (2014) 382–409.

[4] F.J. Mayer, J.R. Reitz, Electromagnetic composites at the Compton scale, Int. J. Theor. Phys. 51 (2012) 322, arXiv:1110.0034.

[5] B.T. Draine, Interstellar dust models: extinction, absorption and emission, in: F. Boulange, C. Joblin, A. Jones, S. Madden (Eds.), Interstellar Dust from

2405-8440/$ – see front matter © 2015 The Author. Published by Elsevier Ltd. This is an open access article under the CC BY-NC-ND license (http://creativecommons.org/licenses/by-nc-nd/4.0/).

Astronomical Observations to Fundamental Studies, in: EAS Publications Series, vol. 35, 2009, pp. 245–268.

[6] B.D. Savage, J.S. Mathis, Observed properties of interstellar dust, Annu. Rev. Astron. Astrophys. 17 (1979) 73–111.

[7] C.F. Bohren, D.R. Huffman, Absorption and Scattering of Light by Small Particles, John Wiley & Sons, New York, 1983.

[8] E.L. Fitzpatrick, D. Massa, An analysis of the shapes of ultraviolet extinction curves. I. The 2175 A bump, Astrophys. J. 307 (1986) 286–294.

[9] G.B. Rybicki, A.P. Lightman, Radiative Processes in Astrophysics, John Wiley & Sons, New York, 1979, p. 289.

[10] N.W. Evans, in: N. Spooner, V. Kudryavtsev (Eds.), IDM (2002): The 4th International Workshop on the Identification of Dark Matter, World Scientific, 2003, arXiv:astro-ph/0211302 (accessed on 27 July 2013).

[11] J.F. Navarro, C.S. Frenk, S.D.M. White, The structure of Cold Dark Matter Halos, Astrophys. J. 462 (1996) 563.

[12] S. Chandrasekhar, An Introduction to the Study of Stellar Structure, Dover Publications, Inc., 1967.

[13] R. Beck, Galactic and extragalactic magnetic fields: a concise review, Astrophys. Space Sci. Trans. 5 (2009) 43–47.

[14] M.J. Geller, J.P. Huchra, Mapping the Universe, Science 246 (1989) 897–903.

[15] L.D. Landau, E.M. Lifshitz, Mechanics, Pergamon Press, Addison–Wesley Publishing Company, Inc., Reading, Massachusetts, 1960, pg. 35.

[16] D.W. Hogg, Distance measures in cosmology, arXiv:astro-ph/9905116v4, 2000 (accessed on 23 November 2013).

[17] E.L. Wright, Ned Wright's cosmology tutorial, http://www.astro.ucla.edu/~wright/Distances_details.gif, 2013.

2405-8440/$ – see front matter © 2015 The Author. Published by Elsevier Ltd. This is an open access article under the CC BY-NC-ND license (http://creativecommons.org/licenses/by-nc-nd/4.0/).